Validation of a dynamic non-linear grinding circuit model for process control

J. D. le Roux[a,*], C. W. Steyn[b]

[a] *Department of Electrical, Electronic and Computer Engineering, University of Pretoria, Pretoria, South Africa.*
[b] *Anglo American PLC, Johannesburg, South Africa.*

Abstract

A step-wise algebraic routine is used to fit a dynamic non-linear model, specifically developed for process control, to steady-state process data of an industrial single-stage grinding mill circuit. Step-test data from the industrial plant is used to validate the response of the non-linear model. The results indicate that the model provides a qualitatively accurate response of the main process variables. Because the non-linear model parameters can be calculated from steady-state data, it provides an advantage over classical system identification methods as it does not require an expensive and disruptive step-test campaign to develop linear transfer function models. The model is ideal for model-based predictive process control.

Keywords: comminution, grinding mill, modelling, parameter estimation, process control, simulation, validation

1. Introduction

A grinding mill in a comminution circuit is one of the most energy intensive unit operations in a mineral processing plant and contributes significantly to the overall processing cost (Curry et al., 2014). Not only is the grinding mill the main bottleneck of the plant, the efficiency of the mill has a significant impact on the final throughput and product quality of the plant (McIvor and Finch, 1991; Sosa-Blanco et al., 2000; Pérez-García et al., 2018). Although throughput and product quality are inversely proportional, advanced process control can improve these competing objectives while optimising the overall energy usage (Bauer and Craig, 2008; Le Roux and Craig, 2019).

Numerous studies confirm the significant benefit advanced process control such as linear model predictive control (MPC) provide to the operation of grinding mill circuits (Niemi et al., 1997; Pomerleau et al., 2000; Ramasamy et al., 2005; Chen et al., 2007; Apelt and Thornhill, 2009; Remes et al., 2010; Yang et al., 2010; Steyn and Sandrock, 2013; Bengtsson et al., 2017). In general, step-test campaigns provide the necessary data for classical system identification tools to develop linear transfer function models for the linear MPC controllers. However, these transfer function models are limited to the operating condition of the plant during the step-test campaign. In addition, since the grinding mill circuit is subject to disturbances in the composition and properties of the raw ore, the linear models must be updated frequently to adapt to the change in operating conditions (Hodouin, 2011; Zhou et al., 2016).

Because of the non-linear nature of the grinding mill process, it is preferable to make use of non-linear models as part of a non-linear MPC supervisory controller (Coetzee et al., 2010; Salazar et al., 2014). The advantage of non-linear models is that they cover a larger range of operating conditions, specifically the parabolic nature of the mill power draw in relation to the mill filling (Apelt et al., 2002; Morrell, 2004; Salazar et al., 2009; Hinde and Kalala, 2009; Le Roux et al., 2020). However, many of the available fundamental non-linear models are not necessarily suitable for implementation in an industrial process controller. The models contain large state and parameter vectors which are difficult to estimate and update from routine operating data (Hodouin, 2011; Zhou et al., 2016; Le Roux et al., 2017).

The non-linear dynamic grinding mill circuit model by Le Roux et al. (2013) uses as few states and parameters as necessary to produce a qualitatively accurate process response. The model appears in a variety simulation studies to test process controllers and process monitoring methods (Olivier and Craig, 2013; Le Roux et al., 2016; Aguila-Camacho et al., 2017; Botha et al., 2018; Wakefield et al., 2018). As shown by Brooks et al. (2021), the model of Le Roux et al. (2013) provides similar predictive performance to linear transfer function models developed from industrial process data. However, because neither Le Roux et al. (2013) nor Brooks et al. (2021) provide a detailed and systematic approach to fit the non-linear model to process data (Pérez-García et al., 2020), the model has not yet been used in an industrial model-based process controller.

The main contribution of this paper is the description of a step-wise procedure to calculate the states and parameters of the non-linear dynamic model in Le Roux et al. (2013) from process data. This will enable the use of the model as part of an industrial model-based predictive controller such as non-linear MPC. The step-wise procedure

*Corresponding author.
Email address: `derik.leroux@up.ac.za` (J. D. le Roux)

to calculate the states and parameters requires only the steady-state process data and does not require expensive step-test data. The model is fitted to steady-state process data from an industrial circuit and the dynamic response of the model is validated against dynamic step-test data from the circuit. Although Le Roux et al. (2013) validated the model, this was only against steady-state process data. This paper improves the validation of the model with the use of dynamic data.

The paper is organized as follows: Section 2 presents the model of the process, Section 3 describes the parameter fitting procedure of the model, Section 4 gives a brief overview of the step-test data as provided by the plant and shows the model validation results, and Section 5 concludes the paper.

2. Process Description and Model

2.1. Process Description

The primary grinding mill circuit in Fig. 1 represents a single stream platinum-group metals concentrator in the Limpopo province of South Africa. Table 1 lists the manipulated variables and measured variables. The manipulated variables are indicated by $u_{\square}$ and the measured variables by $y_{\square}$ where $\square$ represents the subscript. To maintain a degree of consistency between articles the subscripts are related to the variable names in Le Roux et al. (2013). The measured variables are common to most industrial grinding mill circuits (Wei and Craig, 2009).

The primary milling circuit comprises of a 26' radius × 28' length ball mill and a variable speed drive (VSD). The feed of mined ore into the mill (u_{MFO}) (t/h) is controlled by a proportional, integral, derivative (PID) controller that cascades to a VSD feeder under the stockpile silo. Water into the mill is controlled as a ratio to the mill

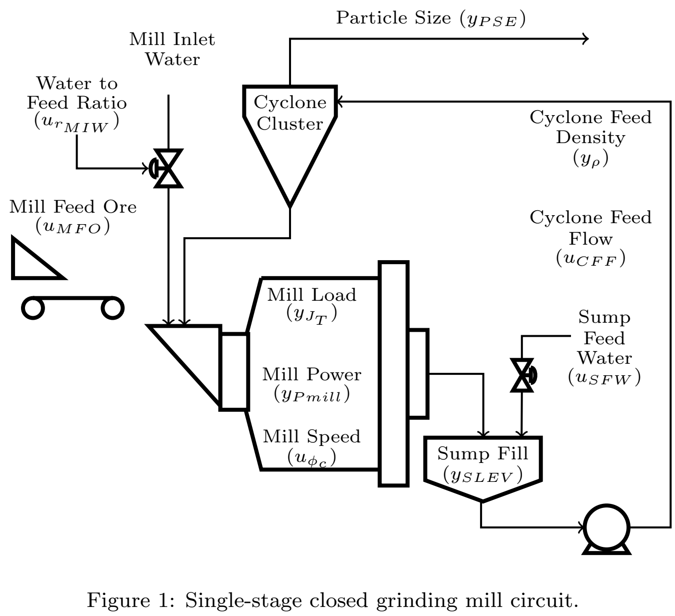

Figure 1: Single-stage closed grinding mill circuit.

feed ore ($u_{r_{MIW}}$) cascading from a ratio controller to a mill inlet water PID controller.

The fractional filling of the mill is given by y_{J_T}. Although the mill filling is not measured directly at most plants, Powell et al. (2009) indicate how y_{J_T} can be calibrated to either load cell or bearing pressure measurements at industrial plants.

The power draw is given by y_{Pmill} (MW). The rotational rate u_{RPM} (rpm) of the mill is converted to the fraction of the critical mill speed (Apelt et al., 2001):

$$u_{\phi_c} = u_{RPM} \frac{2\pi}{60} \sqrt{\frac{D/2}{g}},$$

where D (m) is the internal mill diameter and g (m/s^2) is the gravitational constant. The critical speed is where the angular acceleration equals the gravitational force.

The mill discharges through a partial overflow mechanism into the discharge sump. Pebbles are removed by means of a pebble screen. The slurry in the sump is diluted with water (u_{SFW}) (m^3/h). The level of the sump filled with slurry is given by y_{SLEV} (m^3). The sump content is pumped to a cluster of cyclones via a variable speed pump. The sump discharge density, i.e., the cyclone feed density, is represented by y_ρ (t/m^3). The cumulative flow of feed to the cyclone cluster is represented by u_{CFF} (m^3/h). The cyclone cluster underflow returns to the mill and the overflow reports to the downstream rougher flotation circuit. The final product particle size estimate passing 75 μm (y_{PSE}) at the cyclone overflow is measured by an analyser.

The advanced process control strategy for the grinding mill circuit includes a layered approach consisting of PID, fuzzy-logic-based and model predictive control, as described in Steyn et al. (2010).

2.2. Process Model

The grinding mill circuit in Fig. 1 is modelled with an adapted version of the continuous time phenomenological non-linear population balance model of Le Roux et al. (2013). A brief overview of the model is given below.

For the model, *rocks* refer to all the ore too large to discharge via the discharge mechanism and which must be broken further. *Solids* refer to all ore small enough to discharge via the discharge mechanism from the mill. *Fines* refer to the broken ore below the specification size. Whereas solids are all ore small enough to discharge from the mill, fines are the portion of solids smaller than the specification size. Therefore, solids can be regarded as a combination of fine ore and coarse ore where coarse ore is the portion of solids larger than the specification size.

Table 2 lists the model parameters (cf. Le Roux et al. (2013)). Table 3 provides a description of the lower case subscripts for model flow-rates Q (m^3/h) and model states x (m^3). The first subscript indicates the circuit unit (mill, sump, cyclone) and the second subscript specifies the model

Table 1: Manipulated and measured variables in the primary milling circuit.

Variable	Unit	Description
Manipulated Variables		
u_{MFO}	t/h	Mill feed ore
$u_{r_{MIW}}$	-	Ratio of mill inlet water to feed ore ratio
u_{ϕ_c}	-	Fraction of critical mill speed
u_{SFW}	m^3/h	Sump feed water
u_{CFF}	m^3/h	Cyclone feed flow-rate
Measured Variables		
y_{J_T}	-	Fraction of mill filled with charge
y_{Pmill}	MW	Power draw of the mill
y_{PSE}	%	Product particle size $< 75\mu$m estimate
y_ρ	t/m^3	Sump discharge density
y_{SLEV}	%	Sump slurry fill level

state (rocks, solids, coarse, fines, or water). For flow-rates the third subscript indicates an inflow, outflow or underflow.

2.2.1. Mill Model

Four states describe the population volume balance of the mill: water (x_{mw}), solids (x_{ms}), rocks (x_{mr}), and fines (x_{mf}) (m^3):

$$\frac{d}{dt}x_{mw} = \frac{u_{r_{MIW}}u_{MFO}}{\rho_w} - Q_{mwo} + Q_{cwu} \tag{1a}$$

$$\frac{d}{dt}x_{ms} = (1-\alpha_r)\frac{u_{MFO}}{\rho_o} - Q_{mso} + Q_{csu} + Q_{RC} \tag{1b}$$

$$\frac{d}{dt}x_{mr} = \alpha_r\frac{u_{MFO}}{\rho_o} - Q_{RC} \tag{1c}$$

$$\frac{d}{dt}x_{mf} = \alpha_f\frac{u_{MFO}}{\rho_o} - Q_{mfo} + Q_{cfu} + Q_{FP} \tag{1d}$$

where α_f and α_r represent the fraction of fines and rocks in u_{MFO} respectively, ρ_o and ρ_w (t/m^3) are the ore and water density respectively, Q_{mwo}, Q_{mso}, and Q_{mfo} (m^3/h) are the mill discharge of water, solids, and fines respectively, Q_{cwu}, Q_{csu}, and Q_{cfu} (m^3/h) are the cyclone underflow of water, solids and fines respectively, Q_{RC} (m^3/h) is a rock consumption terms that indicates the volumetric rate of rocks broken into solids, and Q_{FP} (m^3/h) is a fines production term that indicates the volumetric rate of ore broken into fines.

Table 2: Model parameters.

Parameter	Unit	Description
Densities		
ρ_b	t/m^3	Density of balls
ρ_{mc}	t/m^3	Density of mill charge
ρ_o	t/m^3	Density of ore
ρ_w	t/m^3	Density of water
Mill parameters		
α_f	-	Mass fraction of fines in the feed ore
α_r	-	Mass fraction of rocks in the feed ore
δ_s	-	Power parameter for fraction solids in the mill
δ_v	-	Power parameter for volume of mill filled
d_q	h^{-1}	Discharge rate
ε_0	-	Maximum fraction of solids by volume slurry at zero slurry flow
ε_p	-	Porosity of the mill charge
φ_N	-	Rheology normalisation factor
J_B	-	Fraction of mill filled with steel balls
$J_{TP_{max}}$	-	Fraction of mill filled at maximum power draw
K_{FP}	MWh/t	Fines production factor
$K_{FP_{JT}}$	-	Fractional change in fines production factor per change in fractional mill filling
K_{RC}	MWh/t	Rock consumption factor
P_{max}	MW	Maximum mill power draw
S	-	Mill discharge volumetric solids content
U	-	Voidage in the mill charge
v_{mill}	m^3	Mill volume
Sump parameters		
v_{sump}	m^3	Sump volume
Cyclone parameters		
α_{su}	-	Parameter related to fraction solids in cyclone underflow
$C_{1,2,3}$	-	Cyclone model constants
ε_c	m^3/h	Parameter related to coarse split at cyclone

The mill discharge flow-rates in (1) are defined as:

$$Q_{mwo} = \varphi d_q x_{mw}\left(\frac{x_{mw}}{x_{ms}+x_{mw}}\right) \tag{2a}$$

$$Q_{mso} = \varphi d_q x_{mw}\left(\frac{x_{ms}}{x_{ms}+x_{mw}}\right) \tag{2b}$$

$$Q_{mfo} = \varphi d_q x_{mw}\left(\frac{x_{mf}}{x_{ms}+x_{mw}}\right), \tag{2c}$$

Table 3: Description of state and flow-rate lower case subscripts.

Subscript	Description
$x_{\square -}$	m-mill; s-sump; c-cyclone
$x_{-\square}$	w-water; s-solids; c-coarse; f-fines; r-rocks
$Q_{--\square}$	i-inflow; o-outflow; u-underflow

where d_q (1/h) is the discharge rate. Parameter d_q is a fitting parameter to account for the discharge mechanism design (Latchireddi and Morrell, 2003a,b). It represents the pressure or driving force applied to the slurry to discharge from the mill.

The rheology factor φ in (2) is an empirically defined function that incorporates the effect of the fluidity and density of the slurry on the performance of the mill:

$$\varphi = \begin{cases} \sqrt{1 - \left(\varepsilon_0^{-1} - 1\right) \frac{x_s}{x_w}}; & \frac{x_s}{x_w} \leq \left(\varepsilon_0^{-1} - 1\right)^{-1} \\ 0; & \frac{x_s}{x_w} > \left(\varepsilon_0^{-1} - 1\right)^{-1}, \end{cases} \tag{3}$$

where $\varepsilon_0 = 0.60$ is the approximate maximum fraction of solids by volume of slurry at zero slurry flow (Song et al., 2008). The slurry consists only of water for $\varphi = 1$ when $\frac{x_{ms}}{x_{mw}} = 0$. The slurry is a non-flowing mud for $\varphi = 0$ when $\frac{x_{ms}}{x_{mw}} = 1.5$.

Rock consumption (Q_{RC}) and fines production (Q_{FP}) in (1) are defined as:

$$Q_{RC} = \frac{x_{mr} y_{Pmill}}{\rho_o K_{RC} \left(x_{mr} + x_{ms}\right)} \tag{4a}$$

$$Q_{FP} = \frac{y_{Pmill}}{\rho_o K_{FP} \left(1 + K_{FP_{JT}} \left(y_{J_T} - J_{TP_{max}}\right)\right)}, \tag{4b}$$

where K_{RC} (MWh/t) is the rock consumption factor and indicates the energy required per tonne of rocks broken, and K_{FP} (MWh/t) is the fines production factor and indicates the energy required per tonne of fines produced (cf. Amestica et al. (1996) and Hinde and Kalala (2009)). The fractional change in power per fines produced per change in fractional filling of the mill $K_{FP_{JT}}$ is used to modify the fines production factor.

The fraction of the mill filled with charge (y_{J_T}) is defined as:

$$y_{J_T} = \frac{x_{mw} + x_{ms} + x_{mr} + x_{mb}}{v_{mill}}, \tag{5}$$

where v_{mill} (m^3) is the total internal volume of the mill and x_{mb} is the volume of balls in the mill. Although there are various ways to describe steel ball consumption in mills (Apelt et al., 2002; Salazar et al., 2009; Le Roux et al., 2013), because of the slow dynamic change in x_{mb} compared to the other mill states it is assumed x_{mb} is constant.

The mill power draw (y_{Pmill}) (MW) in (4) is modelled as:

$$\begin{aligned} y_{Pmill} = \; & P_{max} u_{\phi_c} \times \\ & \left(1 - \delta_v \left(\frac{y_{J_T}}{J_{TP_{max}}} - 1\right)^2 - \delta_s \left(\frac{\varphi}{\varphi_N} - 1\right)^2\right), \end{aligned} \tag{6}$$

where δ_v is the power change parameter for volume of mill filled, δ_s is the power change parameter for the volume fraction of solids in the slurry, φ_N is a rheology normalisation factor, $J_{TP_{max}}$ is the fraction of the mill filled at maximum power draw, and P_{max} is the maximum mill power draw. If the general grind curve trends are know from historical plant data, P_{max} (MW) and $J_{TP_{max}}$ can each be parameterized as polynomial functions of u_{ϕ_c} (Van der Westhuizen and Powell, 2006; Le Roux et al., 2020).

The mill charge density ρ_{mc} (t/m^3) is given by (cf. Apelt et al. (2001)):

$$\rho_{mc} = \rho_o(1-\varepsilon_p+\varepsilon_p US)+\frac{J_B}{y_{J_T}}(\rho_b-\rho_o)(1-\varepsilon_p)+\varepsilon_p U(1-S), \tag{7}$$

where ε_p is the porosity of the mill charge, J_B is the fraction of the mill filled with steel balls, U is the fraction of grinding media voidage occupied by the slurry, and S is the mill discharge volumetric solids content.

2.2.2. Sump Model

Three states describe the population volume balance of the sump: water (x_{sw}), solids (x_{ss}), and fines (x_{sf}):

$$\frac{d}{dt} x_{sw} = Q_{mwo} - Q_{swo} + u_{SFW} \tag{8a}$$

$$\frac{d}{dt} x_{ss} = Q_{mso} - Q_{sso} \tag{8b}$$

$$\frac{d}{dt} x_{sf} = Q_{mfo} - Q_{sfo}, \tag{8c}$$

where Q_{swo}, Q_{sso} and Q_{sfo} (m^3/h) are the sump discharge flow-rates, solids and fines respectively. It is assumed the slurry in the sump is fully mixed. Since it is assumed the rocks and balls do not exit through the discharge mechanism of the mill, they do not form part of the volume balance of the sump.

The sump discharge is pumped to the cyclone cluster via a variable speed pump. The sump discharge flow-rates in (8) are defined as:

$$Q_{swo} = u_{CFF} \left(\frac{x_{sw}}{x_{sw} + x_{ss}}\right) \tag{9a}$$

$$Q_{sso} = u_{CFF} \left(\frac{x_{ss}}{x_{sw} + x_{ss}}\right) \tag{9b}$$

$$Q_{sfo} = u_{CFF} \left(\frac{x_{sf}}{x_{sw} + x_{ss}}\right). \tag{9c}$$

The percentage of the sump filled with slurry (y_{SLEV}) (%) and the sump outflow density (y_ρ) (t/m^3) are defined as:

$$y_{SLEV} = 100\left(\frac{x_{ss}+x_{sw}}{v_{sump}}\right) \tag{10}$$

$$y_\rho = \frac{\rho_w Q_{swo} + \rho_o Q_{sso}}{Q_{swo}+Q_{sso}} \tag{11}$$

where v_{sump} (m^3) is the physical volume of the sump.

2.2.3. Cyclone Cluster Model

The cyclone cluster is modelled as a single classifier. If needed, the model can be expanded into separate smaller cyclones as in Botha et al. (2018). The aim here is simply to calculate the total water, solids, and fines split at the cluster.

The non-linear static cyclone model presented here aims to model the product size and density by taking the effects of angular velocity of the particle inside the cyclone, the slurry density and slurry viscosity into account. The underflow of coarse material (Q_{ccu}) (m^3/h) is modelled as:

$$\begin{aligned} Q_{ccu} = \quad & \left(Q_{sso}-Q_{sfo}\right)\left(1 - C_1 \exp\left(\tfrac{-u_{CFF}}{\varepsilon_c}\right)\right)\times \\ & \left(1-\left(\tfrac{F_i}{C_2}\right)^{C_3}\right)\left(1-P_i^{C_3}\right), \end{aligned} \tag{12}$$

where $F_i = \frac{Q_{sso}}{u_{CFF}}$ is the fraction solids in the cyclone feed, $P_i = \frac{Q_{sfo}}{Q_{sso}}$ is the fraction fines in the feed solids, ε_c (m^3/h) relates to the coarse split, $C_1 = 0.70$ relates to the split at low-flows when the centrifugal force on particles is relatively small, $C_2 = 0.70$ normalizes the fraction solids in the feed according to the upper limit for the packing fraction of solid particles, and C_3 is an integer which adjusts the sharpness of the dependency on F_i and P_i.

The fraction of solids in the underflow (F_u) can be expressed per definition as:

$$F_u = \frac{Q_{csu}}{Q_{csu}+Q_{cwu}}. \tag{13}$$

This can be modelled as follows to determine the amount of water and fines accompanying the coarse underflow:

$$F_u = C_2 - (C_2 - F_i)\exp\left(-\frac{Q_{ccu}}{\alpha_{su}\varepsilon_c}\right), \tag{14}$$

where α_{su} relates to the fraction solids in the underflow.

The ratio of fines to water in the feed and underflow respectively can be regarded as approximately equal if it is assumed the fines are not influenced by centrifugal forces, i.e., $\frac{Q_{sfo}}{Q_{swo}} \approx \frac{Q_{cfu}}{Q_{cwu}}$. Consequently, using (13), the cyclone underflow flow-rates in (1) can be expressed as:

$$Q_{cwu} = \frac{Q_{swo}\left(Q_{ccu}-F_u Q_{ccu}\right)}{F_u Q_{swo} + F_u Q_{sfo} - Q_{sfo}} \tag{15a}$$

$$Q_{cfu} = \frac{Q_{sfo}\left(Q_{ccu}-F_u Q_{ccu}\right)}{F_u Q_{swo} + F_u Q_{sfo} - Q_{sfo}} \tag{15b}$$

$$Q_{csu} = Q_{ccu} + Q_{cfu}. \tag{15c}$$

The cyclone water overflow (Q_{cwo}), solids overflow (Q_{cso}), and fines overflow (Q_{cfo}) can be calculated using a flow balance around the cyclone.

The product particle size passing the specification size of 75 μm (y_{PSE}) is defined as:

$$y_{PSE} = 100\left(\frac{Q_{cfo}}{Q_{cso}}\right). \tag{16}$$

2.3. State space Representation

A state-space model of the grinding mill circuit can be formulated as:

$$\begin{aligned} \tfrac{d}{dt}\mathbf{x} &= \mathbf{f}\left(t,\mathbf{x},\mathbf{u},\mathbf{p}\right) \\ \mathbf{y} &= \mathbf{h}\left(t,\mathbf{x},\mathbf{u},\mathbf{p}\right), \end{aligned} \tag{17}$$

where $\mathbf{x} = \left[x_{mw}, x_{ms}, x_{mr}, x_{mf}, x_{sw}, x_{ss}, x_{sf}\right]^T$ are the states, $\mathbf{u} = \left[u_{MFO}, u_{r_{MIW}}, u_{\phi_c}, u_{SFW}, u_{CFF}\right]^T$ are the inputs, $\mathbf{y} = \left[y_{J_T}, y_{Pmill}, y_{SLEV}, y_\rho, y_{PSE}\right]^T$ are the outputs, and $\mathbf{p}$ contains the model parameters as listed in Table 2. Function $\mathbf{f}(\cdot)$ is given by (1) and (8), and function $\mathbf{h}(\cdot)$ by (5), (6), (10), (11), and (16).

3. Step-wise Parameter Estimation Procedure

The aim of this section is to describe a step-wise procedure to determine the model parameters $\mathbf{p}$ for the system model in (17) from steady-state process data, i.e., where $\frac{d}{dt}\mathbf{x} = \mathbf{0}$ in (17). A consequence is that the model states $\mathbf{x}$ at the steady-state of operation is also determined.

The variables as listed in Table 1 are assumed to be known at the start of the estimation procedure:

- Manipulated variables:
  u_{MFO}, $u_{r_{MIW}}$, u_{ϕ_c}, u_{SFW}, and u_{CFF}
- Measured variables:
  y_{J_T}, $y_{P_{mill}}$, y_{PSE}, y_ρ, and y_{SLEV}

The variables listed above represent the minimum set of real-time process variable measurements necessary to determine the model states and parameters. These variables are insufficient for a mass or volume balance around the circuit. The estimation procedure can be completed even if these measurements are not entirely accurate, but any water or solids that is unaccounted for will cause poor model prediction. It is generally most visible in the model prediction of y_{SLEV} which will either increase or decrease sharply based on an unmeasured disturbance such as spillage water. Therefore, it is important that measurement instrumentation is maintained well and calibrated to produce accurate and trustworthy measurements.

The following parameters are assumed to be available from sampling campaign data or operator knowledge:

- Densities: ρ_b, ρ_o, and ρ_w
- Feed distribution: α_f and α_r

- Mill charge: J_B, ρ_{mc}, and U
- Power draw: J_{TPmax} and P_{max}
- Volumes: v_{mill} and v_{sump}

If the feed distribution is not measured on-line (Maritz et al., 2019), a general estimate is sufficient. Similarly, the mill charge parameters will not necessarily be known exactly and a general estimate can be used (Napier-Munn et al., 2005).

As mentioned in Section 2.2.1, if grind curves can be generated based on historical data, P_{max} and J_{TPmax} can be parameterized as polynomial functions of u_{ϕ_c} using a least squares fit. If this is not the case, P_{max} is the power draw for the specific operating condition. Similarly, the operators should know whether the mill is operating before or past the peak in power in terms of y_{J_T}. In the case where the mill operates before the peak in power, $J_{TPmax} \geq y_{J_T}$. Otherwise, $J_{TPmax} \leq y_{J_T}$.

Finally, the following parameters are degrees of freedom that need to be specified: C_3, φ_N, $K_{FP_{JT}}$.

3.1. Sump

The aim of this subsection is to calculate steady-state values for x_{sw} and x_{ss} in (9a) and (9b).

If the total mass of slurry in the sump is given by $M_T = M_S + M_W$ where M_S is the mass of solids and M_W is the mass of water, the flow of material exiting the sump ($u_{CFF} = M_T/y_\rho$) can be written as:

$$\frac{M_T}{y_\rho} = \frac{M_S}{\rho_o} + \frac{M_W}{\rho_w}. \tag{18}$$

Eq. (18) can be simplified to give the solid mass fraction:

$$\frac{M_S}{M_T} = \frac{\frac{1}{y_\rho} - 1}{\frac{1}{\rho_o} - 1}. \tag{19}$$

From the results above, the sump water and solids discharge (Q_{swo} and Q_{sso}) and volumes (x_{sw} and x_{ss}) can be calculated from measured variables and parameters:

$$Q_{swo} = \frac{y_\rho u_{CFF}}{\rho_w}\left(1 - \frac{\frac{1}{y_\rho} - 1}{\frac{1}{\rho_o} - 1}\right) \tag{20a}$$

$$Q_{sso} = \frac{y_\rho u_{CFF}}{\rho_o}\left(\frac{\frac{1}{y_\rho} - 1}{\frac{1}{\rho_o} - 1}\right) \tag{20b}$$

$$x_{sw} = \frac{y_\rho y_{SLEV} v_{sump}}{100\rho_w}\left(1 - \frac{\frac{1}{y_\rho} - 1}{\frac{1}{\rho_o} - 1}\right) \tag{20c}$$

$$x_{ss} = \frac{y_\rho y_{SLEV} v_{sump}}{100\rho_o}\left(\frac{\frac{1}{y_\rho} - 1}{\frac{1}{\rho_o} - 1}\right). \tag{20d}$$

3.2. Cyclone Cluster

The aim of this section is to calculate a steady-state value for x_{sf} in (9c), and parameter values ε_c and α_{su} in (12) and (14). The calculations below depend on the states and flows determined in Section 3.1 above.

Given steady-state operation and assuming no unmeasured disturbances in the circuit, the volumetric flow-rate of water and solids exiting the circuit is:

$$Q_{cwo} = \frac{u_{r_{MIW}} u_{MFO}}{\rho_w} + u_{SFW} \tag{21a}$$

$$Q_{cso} = \frac{u_{MFO}}{\rho_o}. \tag{21b}$$

Therefore, from a flow-balance around the cyclone it is possible to determine the water and solids underflow:

$$Q_{cwu} = Q_{swo} - Q_{cwo} \tag{22a}$$

$$Q_{csu} = Q_{sso} - Q_{cso} \tag{22b}$$

Given the underflows in (22) above, the fraction of solids in the underflow (F_u) in (13) can be determined.

Using (15a), set $\beta = \frac{Q_{cwu}}{Q_{swo}}$ such that (15b) can be written as $Q_{cfu} = \beta Q_{sfo}$. Consequently, rewrite (15a) to find Q_{ccu} in terms of β:

$$Q_{ccu} = \frac{\beta F_u Q_{swo} - \beta Q_{sfo}(1 - F_u)}{1 - F_u}. \tag{23}$$

From a flow balance around the cyclone, the fines and solids overflows are given by:

$$Q_{cfo} = Q_{sfo} - Q_{cfu} \tag{24a}$$

$$Q_{cso} = Q_{sso} - Q_{csu} = Q_{sso} - Q_{ccu} - Q_{cfu}. \tag{24b}$$

Finally, using (23)-(24) it is possible to rewrite (16) as:

$$y_{PSE} = 100\left(\frac{Q_{sfo}(1 - \beta)}{Q_{sso} - \frac{\beta F_u Q_{swo} - \beta Q_{sfo}(1 - F_u)}{1 - F_u} - \beta Q_{sfo}}\right). \tag{25}$$

Substituting (9) into (25) and simplifying, x_{sf} can be calculated as:

$$x_{sf} = \frac{F_u y_{PSE} x_{ss} - y_{PSE} x_{ss} + \beta F_u y_{PSE} x_{sw}}{100\,(F_u + \beta - F_u\beta - 1)}. \tag{26}$$

Since x_{sf} is now known, the discharge of fines from the sump in (9c) is:

$$Q_{sfo} = x_{sf} u_{CFF} \frac{100}{y_{SLEV} v_{sump}}. \tag{27}$$

The remaining set of over- and underflows at the cyclone can be calculated as:

$$Q_{ccu} = \frac{\beta u_{CFF}}{x_{ss} + x_{sw}}\left(\frac{x_{sw} F_u + x_{sf}(F_u - 1)}{1 - F_u}\right) \tag{28a}$$

$$Q_{cfu} = \frac{x_{sf}(Q_{ccu} - F_u Q_{ccu})}{F_u x_{sw} + F_u x_{sf} - x_{sf}} \tag{28b}$$

$$Q_{cfo} = Q_{cso}\frac{y_{PSE}}{100}. \tag{28c}$$

Finally, given the flow-rates and states above, it is possible to calculate the cyclone parameters ε_c and α_{su}:

$$\varepsilon_c = -\frac{u_{CFF}}{\log(\lambda)} \tag{29a}$$

$$\alpha_{su} = -\frac{Q_{ccu}}{\varepsilon_c \log(\frac{C_2-F_u}{C_2-F_i})} \tag{29b}$$

where

$$\lambda = \frac{1}{C_1} - \frac{Q_{ccu}}{C_1(Q_{sso}-Q_{sfo})(1-(F_i/C_2)^{C_3})(1-P_i^{C_3})}.$$

Note, $C_1 = C_2 = 0.7$ is known *a-priori* as defined in Section 2.2.3. Unless further measurements of the cyclone underflow are available, C_3 cannot be fitted to data. Subsequently, C_3 is a degree of freedom that is heuristically chosen as the smallest positive integer for which both ε_c and α_{su} are positive. The choice of C_3 does not influence the parameters for the grinding mill.

3.3. Mill

The aim of this section is to calculate steady-state values for x_{mw}, x_{ms}, x_{mf}, x_{mr}, and x_{mb}, the discharge rate d_q, the power draw parameters δ_v and δ_s, and the breakage parameters K_{FP}, and K_{RC}. The calculations below depend on the states and flows determined in Sections 3.1 and 3.2 above.

3.3.1. Mill States and Discharge

From a mass balance around the sump at steady-state, the mill discharge flow-rates are:

$$Q_{mwo} = Q_{swo} - u_{SFW} \tag{30a}$$

$$Q_{mso} = Q_{sso} \tag{30b}$$

$$Q_{mfo} = Q_{sfo} \tag{30c}$$

It is assumed that general estimates of the mill charge density (ρ_{mc}), charge voidage (U), and fraction of mill filled with steel balls (J_B) are available from sampling campaign data or operator knowledge. Therefore, the charge porosity (ε_p) can be calculated from (7) as:

$$\varepsilon_p = \frac{\rho_{mc} - \rho_o - (\rho_b - \rho_o)J_B/y_{J_T}}{\rho_o US - \rho_o + (\rho_b - \rho_o)J_B/y_{J_T} + U(1-S)}, \tag{31}$$

where $S = \frac{Q_{mso}}{Q_{mso}+Q_{mwo}}$. Subsequently, the mill states in (1) can be determined in the following order as:

$$x_{mb} = \left(1-\varepsilon_p\right) J_B v_{mill} \tag{32a}$$

$$x_{mw} = (1-S)\,\varepsilon_p U y_{J_T} v_{mill} \tag{32b}$$

$$x_{ms} = S\varepsilon_p U y_{J_T} v_{mill} \tag{32c}$$

$$x_{mf} = \left(\frac{Q_{mfo}}{Q_{mso}}\right) x_{ms} \tag{32d}$$

$$x_{mr} = y_{J_T} v_{mill} - x_{mb} - x_{mw} - x_{ms}. \tag{32e}$$

Given the mill state values calculated above, the discharge rate d_q can be calculated from (2) as:

$$d_q = Q_{mwo}\left(\frac{x_{mw}+x_{ms}}{\varphi x_{mw}^2}\right) \tag{33}$$

where φ is given in (3).

3.3.2. Mill power draw

Assuming $\delta_v = \delta_s$, these parameters can be calculated from (6) as follows:

$$\delta_s = \delta_v = \frac{1 - \frac{y_{Pmill}}{P_{max} u_{\phi_c}}}{\left(\frac{y_{J_T}}{J_{TPmax}} - 1\right)^2 + \left(\frac{\varphi}{\varphi_N} - 1\right)^2}. \tag{34}$$

If sufficient process data is available to evaluate the impact of the solids to water ratio on the power draw of the mill (Steyn and Sandrock, 2013), it is possible to determine an accurate estimate of φ_N. Otherwise, φ_N is a degree of freedom that needs to be chosen. A conservative choice is $\varphi_N = 0.70$ which corresponds to $\frac{x_{ms}}{x_{mw}} \approx 0.75$.

3.3.3. Breakage rates

Since steady-state is assumed, the breakage rates in (4a) and (4b) can be back-calculated from (1c) and (1d) respectively:

$$K_{RC} = \frac{y_{Pmill} x_{mr}}{u_{MFO}\alpha_r\left(x_{mr}+x_{ms}\right)} \tag{35a}$$

$$K_{FP} = \frac{y_{Pmill}}{\rho_o\left(1 + K_{FP_{JT}}\left(y_{J_T} - J_{TP_{max}}\right)\right)} \times \frac{1}{\left(Q_{mfo} - Q_{cfu} - \frac{u_{MFO}\alpha_f}{\rho_o}\right)}, \tag{35b}$$

where $K_{FP_{JT}}$ is a degree of freedom to adjust the breakage rate of fines given the variation in y_{J_T}. Unless historic data is available to fit $K_{FP_{JT}}$, it can be set to $K_{FP_{JT}} = 0$. If $y_{J_T} = J_B$, then $x_{mr} \approx 0$ in (32). In this case it is necessary to modify the rock consumption term in (4a) such that $Q_{RC} = \frac{y_{Pmill}}{\rho_o K_{RC}}$.

3.4. Summary

The procedure to calibrate the model is summarized in Fig. 2. The estimation procedure is divided into three phases starting at the top with the sump, followed by the cyclone, and ending at the grinding mill. Information calculated in one phase is passed to the next. For each phase the set of known variables and parameters necessary to complete the calibration is shown on the far left, the set of calculations needed to calibrate the model in the centre, and the final calibrated model parameters **p** and the model states **x** at the specific steady-state operating condition are shown on the far right.

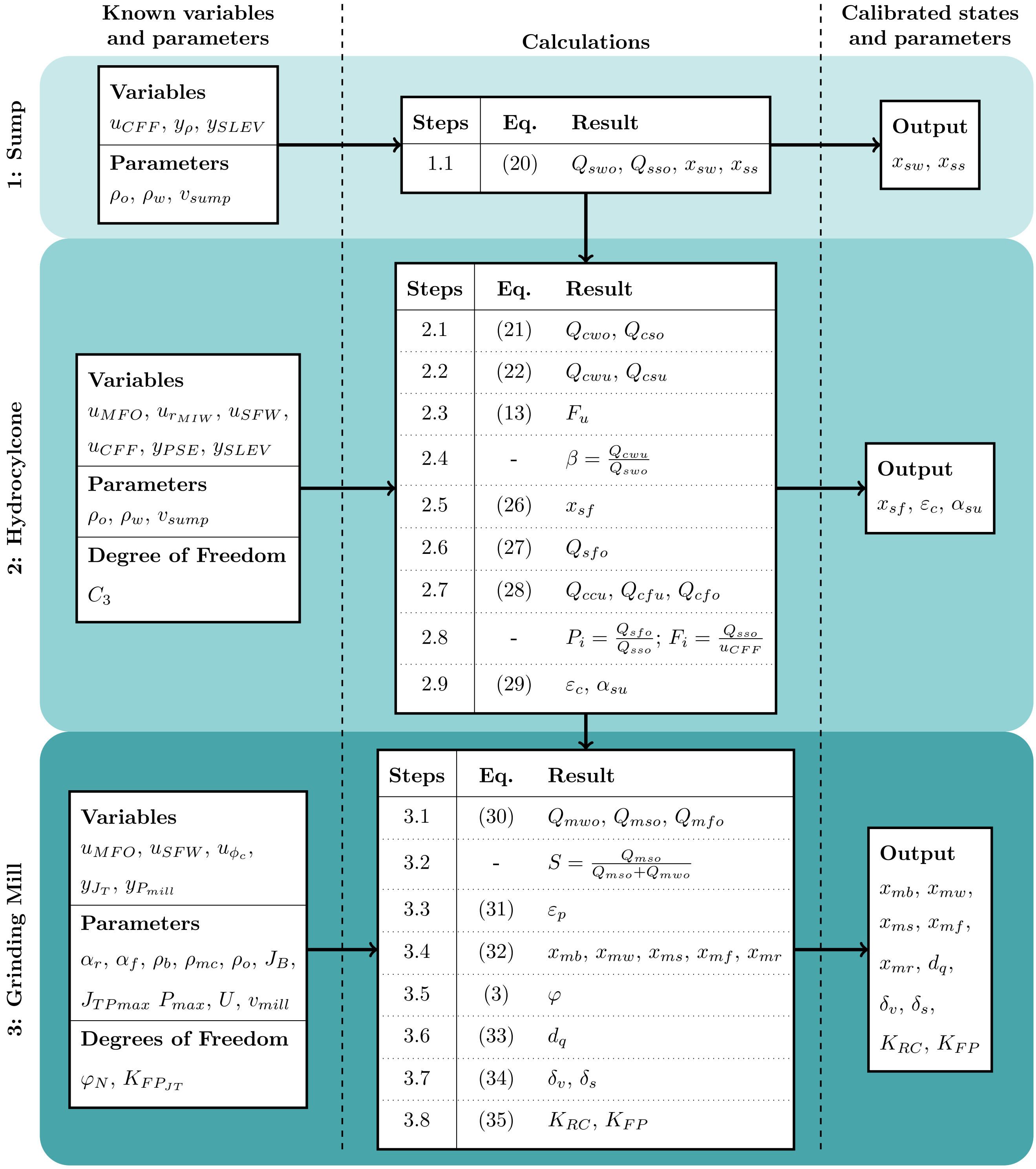

Figure 2: Summary of model calibration process.

4. Validation

4.1. Estimated Parameters from Step-test Data

The model is validated with step-test data from the industrial primary milling circuit illustrated in Fig. 1. Step-tests were performed between the 1st and 3rd February 2020. Data was sampled at a rate of 16.7 mHz (period of 60 s). A section of data of 24 hours with no instrumentation failure or plant stoppages is used for validation of the model. The manipulated variables $\mathbf{u}$ and measured variables $\mathbf{y}$ as in (17) for the specific 24 hour step-test period is shown in Figs. 3 and 4 respectively.

Table 4 shows the steady-state operating condition in

Table 4: Steady-state operating condition and process data.

Variable	Value	Unit
Operating condition		
u_{MFO}	1191	t/h
$u_{r_{MIW}}$	0.572	m^3/h
u_{ϕ_c}	0.768	-
u_{SFW}	870	m^3/h
u_{CFF}	2921	m^3/h
y_{J_T}	0.328	-
$y_{P_{mill}}$	14.8	MW
y_{SLEV}	59.4	%
y_ρ	1.77	t/m^3
y_{PSE}	37.9	%
Process Data		
α_f	0.10	-
α_r	0.50	-
J_B	0.30	-
J_{TPmax}	0.23	-
P_{max}	19.7	MW
ρ_b	7.8	t/m^3
ρ_{mc}	5.55	t/m^3
ρ_o	3.2	t/m^3
ρ_w	1	t/m^3
U	1	-
v_{mill}	540.9	m^3
v_{sump}	345.8	m^3

terms of the manipulated and measured variables at the start of validation period. The table also shows the process data assumed to be known prior to the estimation as available from sampling campaign data. In terms of the power draw parameters J_{TPmax} and P_{max} in Table 4, no historical grind curve data was available to parameterize these parameters as functions of u_{ϕ_c}. However, it was known from the operators that the plant operated past the point where the maximum power was drawn. Therefore, J_{TPmax} was conservatively and heuristically set as $J_{TPmax} = 0.7y_{JT}$. Similarly, P_{max} was set as $P_{max} = 1.02y_{P_{mill}}/u_{\phi_c}$. The 2% increase in $y_{P_{mill}}$ is an increase of 300 kW above the initial steady-state operating condition.

The procedure outlined in Section 3 and summarized in Fig. 2 was followed to fit the model described in Section 2 to the data in Table 4. The calculated parameters and the process states at the specific steady-state operating condition are shown in Table 5.

4.2. Simulated Model

The dynamic model (17) is simulated using the fourth-order Runge-Kutta numerical integration method with a step-size of 60 s. The model takes as input the process data in Table 4, the process parameters and initial state condition in Table 5 and the manipulated variables **u** shown in Fig. 3. The comparison of the output of the model **y** to the measured data is shown in Fig. 4.

At no point during the simulation are any of the model parameters updated. Therefore, once the model is fitted to initial steady-state condition at $t = 0$ h in Figs. 3 and 4, the model response is a pure simulation to be compared with the actual plant response.

Table 5: Parameter and state values calculated according to the step-wise process in Section 3.

Parameter	Value	Unit
Degrees of Freedom		
C_3	4	-
φ_N	0.7	-
$K_{FP_{JT}}$	20	-
Model Parameters		
α_{su}	0.119	-
ε_c	2528	m^3/h
$\delta_v = \delta_s$	0.0911	-
d_q	114.7	h^{-1}
K_{RC}	5.97×10^{-3}	MWh/t
K_{FP}	15.0×10^{-3}	MWh/t
Process States		
x_{mw}	31.0	m^3
x_{ms}	31.1	m^3
x_{mf}	5.22	m^3
x_{mr}	9.84	m^3
x_{mb}	105	m^3
x_{sw}	133	m^3
x_{ss}	72.2	m^3
x_{sf}	12.1	m^3

4.3. Discussion

As seen in Fig. 4, the model is able to capture the main dynamic variations y_{J_T}, $y_{P_{mill}}$, y_ρ, and y_{PSE} over an extended period of time. Because the sump acts as an integrator for the level of the sump filled with slurry (y_{SLEV}), it is not easy to capture its dynamic response with sufficient accuracy. The sharp increase between $t = 15$ h and $t = 24$ h can possibly be attributed to an unmeasured disturbance propagating through the sump. In practice a simple feedback controller can maintain y_{SLEV} within allowable limits.

The model is able to account for the large change in $y_{P_{mill}}$ as a result of the change in u_{ϕ_c} shown in Fig. 3. It is interesting to see that there is not a significant change in y_{J_T} or y_{PSE} for the variation in u_{ϕ_c}. This indicates that

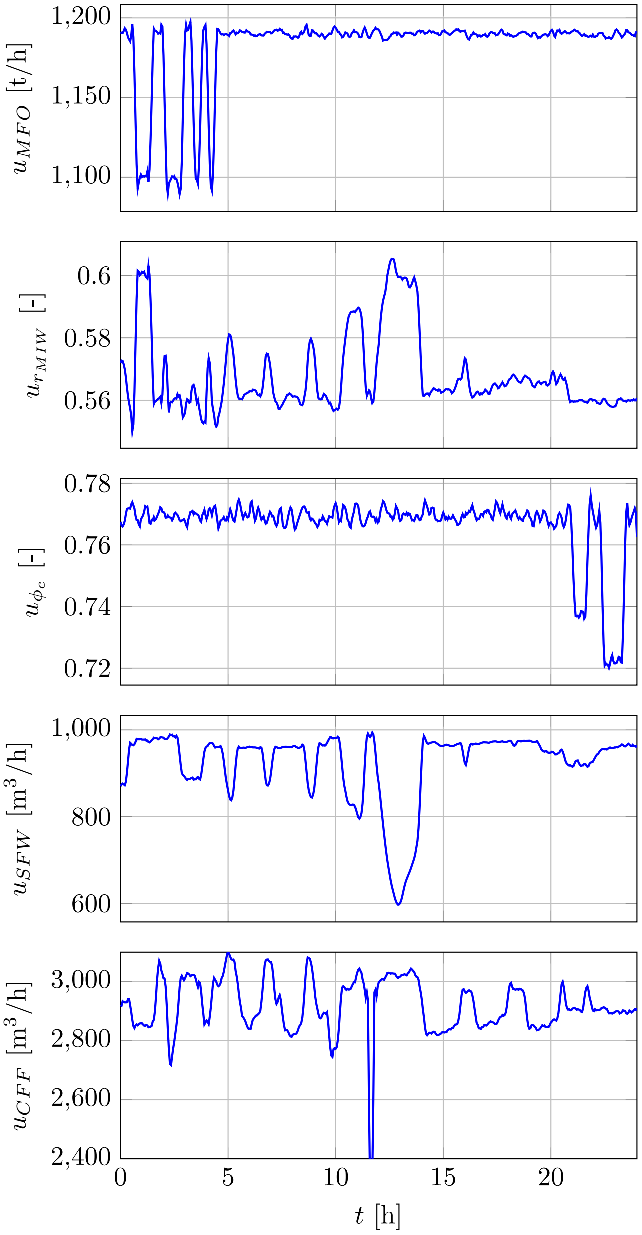

Figure 3: Manipulated variable step-test data.

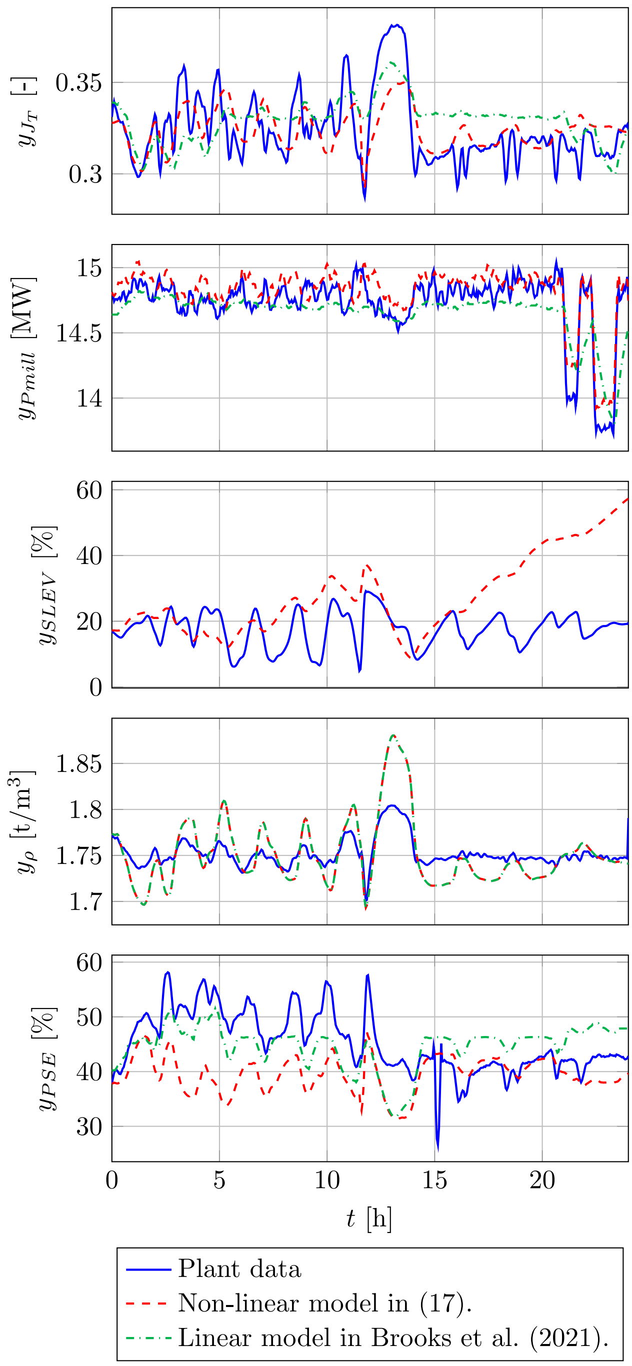

Figure 4: Validation of the model output against the measured plant step-test data.

the charge in the mill is most probably overshooting the toe of the charge and impacting the mill liners.

As seen in Fig. 4, the model provides a filtered response for the various measured variables. Given the simplicity of the model, mismatch between the model and the actual plant response is to be expected. However, as noted by Le Roux et al. (2013), the aim of the model is for process control and does not necessarily intend to produce a quantitatively accurate response. The qualitatively accurate model response is sufficient for a model-based predictive feedback controller such as non-linear MPC (Coetzee et al., 2010; Le Roux et al., 2016; Aguila-Camacho et al., 2017), or for process monitoring purposes (Wakefield et al., 2018). In other words, the plant can be controlled as long as the direction of deviation of a variable can be predicted even though the exact magnitude of the deviation is uncertain. In the case of MPC, the prediction horizon should at least capture the settling time of the plant to ensure the dynamics of the process is represented in any prediction (Seborg et al., 2016). For example, if the settling time of a grinding mill is about an hour the model only needs to be accurate for this time period. The model can be updated once a new steady-state is reached to reduce model plant mismatch (Olivier and Craig, 2013).

Table 6: Statistical comparison of model responses in Fig. 4.

	Non-linear model†		Linear model‡	
	RMSE	R^2	RMSE	R^2
y_{J_T}	0.0157	0.325	0.0177	0.231
y_{Pmill}	0.128	0.849	0.187	0.524
y_{ρ}	0.0240	0.785	0.0241	0.782
y_{PSE}	8.16	0.0420	5.54	0.123

† Non-linear model in (17).

‡ Linear model from Brooks et al. (2021).

Brooks et al. (2021) uses the same set of step-test data to develop linear transfer function models for all the measured variables except y_{SLEV}. The linear model prediction is included in Fig. 4. A statistical comparison of the non-linear and linear model performance in terms of the root mean squared error (RMSE) and the coefficient of determination (R^2) is shown in Table 6. The non-linear model has similar predictive performance than the linear transfer function models. The advantage of the non-linear model presented in this paper is that it requires only the accurate measurement of a single steady-state condition. In contrast, the linear transfer function models require an expensive and disruptive step-test campaign. The linear transfer function model will also remain valid for the specific operating condition, whereas the non-linear model can be fitted to any operating condition.

5. Conclusion

The contribution of this article is a step-wise procedure to fit a non-linear model of a grinding mill circuit to steady-state process data. By way of example, the non-linear model is fitted to process data from an industrial primary milling circuit and is validated against step-test data from the plant. The advantage of the non-linear model is that the model parameters can be calculated from a single steady-state operating condition. It does not require an expensive step-test campaign such as is needed to develop linear transfer function models.

The comparison between the response of the simulated non-linear model and the response of the plant shows that the model provides a sufficiently accurate representation of the dynamics of the process. Specifically, the model is able to capture in a qualitative sense the dynamics of the fraction of the mill filled with charge (y_{J_T}), the power draw (y_{Pmill}), the sump discharge density (y_{ρ}), and the product particle size < 75 μm (y_{PSE}). Therefore, the model is ideally suited for model-based predictive control or for process monitoring for industrial grinding mill circuits. The model parameters can easily be updated for each steady-state operating condition.

Future work will consider automatic derivation of grind curves based on historical data to parameterize the power draw model parameters in terms of mill speed.

Acknowledgement

The authors would like to thank Mr Shaun Johnson from Anglo American Platinum for his assistance with the step-test data.

References

Aguila-Camacho, N., le Roux, J. D., Duarte-Mermoud, M. A., Orcharda, M. E., 2017. Control of a grinding mill circuit using fractional order controllers. J. Process Control 53, 80–94.

Amestica, R., Gonzalez, G. D., Menacho, J., Barria, J., 1996. A mechanistic state equation model for semiautogenous mills. Int. J. Mineral Process. 44-45, 349–360.

Apelt, T. A., Asprey, S. P., Thornhill, N. F., 2001. Inferential measurement of SAG mill parameters. Minerals Eng. 14 (6), 575–591.

Apelt, T. A., Asprey, S. P., Thornhill, N. F., 2002. Inferential measurement of SAG mill parameters II: State estimation. Minerals Eng. 15, 1043–1053.

Apelt, T. A., Thornhill, N. F., 2009. Inferential measurement of SAG mill parameters V: MPC simulation. Minerals Eng. 22, 1045–1052.

Bauer, M., Craig, I. K., 2008. Economic assessment of advanced process control: A survey and framework. J. Process Control 18 (1), 2–18.

Bengtsson, M., Asbjornsson, G., Hulthen, E., Evertsson, M., 2017. Towards dynamical profit optimisation of comminution circuits. Minerals Eng. 103-104, 14–24.

Botha, S., Craig, I. K., Le Roux, J. D., 2018. Hybrid non-linear model predictive control of a run-of-mine ore grinding mill circuit. Minerals Eng. 123, 49–62.

Brooks, K., Le Roux, D., Shardt, Y., Steyn, C., 2021. Comparison of semirigorous and empirical models derived using data quality assessment methods. Minerals 11 (9), 954.

Chen, X., Zhai, J., Li, S., Li, Q., 2007. Application of model predictive control in ball mill grinding circuit. Minerals Eng. 20 (11), 1099–1108.

Coetzee, L. C., Craig, I. K., Kerrigan, E. C., 2010. Robust nonlinear model predictive control of a run-of-mine ore milling circuit. IEEE Trans. Control Syst. Technol. 18 (1), 222–229.

Curry, J. A., Ismay, M. J., Jameson, G. J., 2014. Mine operating costs and the potential impacts of energy and grinding. Minerals Eng. 56, 70–80.

Hinde, A. L., Kalala, J. T., 2009. The application of a simplified approach to modelling tumbling mills, stirred media mills and HPGR's. Minerals Eng. 22 (7-8), 633–641.

Hodouin, D., 2011. Methods for automatic control, observation and optimization in mineral processing plants. J. Process Control 21 (2), 211–225.

Latchireddi, S., Morrell, S., 2003a. Slurry flow in mills: Grate-only discharge mechanism (Part-1). Minerals Eng. 16, 625–633.

Latchireddi, S., Morrell, S., 2003b. Slurry flow in mills: Grate-pulp lifter discharge systems (Part 2). Minerals Eng. 16, 635–642.

Le Roux, J., Craig, I. K., 2019. Plant-wide control framework for a grinding mill circuit. Ind. Eng. Chem. Res. 58 (26), 11585–11600.

Le Roux, J. D., Craig, I. K., Hulbert, D. G., Hinde, A. L., 2013. Analysis and validation of a run-of-mine ore grinding mill circuit model for process control. Minerals Eng. 43-44, 121–134.

Le Roux, J. D., Olivier, L. E., Naidoo, M. A., Padhi, R., Craig, I. K., 2016. Throughput and product quality control for a grinding mill circuit using non-linear MPC. J. Process Control 42, 35–50.

Le Roux, J. D., Steinboeck, A., Kugi, A., Craig, I. K., 2017. An EKF observer to estimate semi-autogenous grinding mill hold-ups. J. Process Control 51, 2741.

Le Roux, J. D., Steinboeck, A., Kugi, A., Craig, I. K., 2020. Steady-state and dynamic simulation of a grinding mill using grind curves. Minerals Eng. 152, 106208.

Maritz, M. G., le Roux, J. D., Craig, I. K., 2019. Feed size distribution feedforward control for a grinding mill circuit. IFAC-PapersOnLine 52 (14), 7–12, 18th IFAC Symposium on Control,

Optimization and Automation in Mining, Mineral and Metal Processing, MMM 2019.
McIvor, R., Finch, J., 1991. A guide to interfacing of plant grinding and flotation operations. Minerals Eng. 4 (1), 9–23.
Morrell, S., 2004. A new autogenous and semi-autogenous mill model for scale-up, design and optimisation. Minerals Eng. 17 (3), 437–445.
Napier-Munn, T. J., Morrell, S., Morrison, R. D., Kojovic, T., 2005. Mineral Communition Circuits: Their Operation and Optimisation, 3rd Edition. JKMRC Monograph Series in Mining and Mineral Processing.
Niemi, A. J., Tian, L., Ylinen, R., 1997. Model predictive control for grinding systems. Control Eng. Practice 5 (2), 271–278.
Olivier, L. E., Craig, I. K., 2013. Model-plant mismatch detection and model update for a run-of-mine ore milling circuit under model predictive control. J. Process Control 23 (2), 100–107.
Pérez-García, E. M., Bouchard, J., Poulin, É., 2018. Integration of a liberation model in a simulation framework for comminution circuits. Minerals Eng. 126, 167–176.
Pérez-García, E. M., Bouchard, J., Poulin, É., 2020. Systematic calibration of a simulated semi-autogenous/ball-mill grinding circuit. IFAC-PapersOnLine 53 (2), 12026–12031.
Pomerleau, A., Hodouin, D., Desbiens, A., Gagnon, E., 2000. A survey of grinding circuit control methods: from decentralized PID controllers to multivariable predictive controllers. Powder Tech. 108 (2-3), 103–115.
Powell, M. S., van der Westhuizen, A. P., Mainza, A. N., 2009. Applying grindcurves to mill operation and optimisation. Minerals Eng. 22 (7-8), 625–632.
Ramasamy, M., Narayanan, S. S., Rao, C. D. P., 2005. Control of ball mill grinding circuit using model predictive control scheme. J. Process Control 15 (3), 273–283.
Remes, A., Aaltonen, J., Koivo, H., 2010. Grinding circuit modeling and simulation of particle size control at Siilinjärvi concentrator. Int. J. Mineral Process. 96 (1-4), 70–78.
Salazar, J., Valdez-Gonzalres, H., Vyhmesiter, E., Cubillos, F., 2014. Model predictive control of semi-autogenous mills. Minerals Eng. 64, 92–96.
Salazar, J. L., Magne, L., Acua, G., Cubillos, F., 2009. Dynamic modelling and simulation of semi-autogenous mills. Minerals Eng. 22 (1), 70–77.
Seborg, D. E., Edgar, T. F., Mellichamp, D. A., Doyle III, F. J., 2016. Process dynamics and control. John Wiley & Sons.
Song, C., Wang, P., Makse, H. A., 2008. A phase diagram for jammed matter. Nature 453 (7195), 629632.
Sosa-Blanco, C., Hodouin, D., Bazin, C., Lara-Valenzuele, C., Salazar, J., 2000. Economic optimisation of a flotation plant through grinding circuit tuning. Minerals Eng. 13 (10-11), 999–1018.
Steyn, C. W., Brooks, K. S., De Villiers, P. G. R., Muller, D., Humphries, G., 2010. A holistic approach to control and optimization of an industrial run-of-mine ball milling circuit. IFAC Proceedings Volumes 43, 137–141.
Steyn, C. W., Sandrock, C., 2013. Benefits of optimisation and model predictive control on a fully autogenous mill with variable speed. Minerals Eng. 53, 113–123.
Van der Westhuizen, A. P. P., Powell, M. S., 2006. Milling curves as a tool for characterising SAG mill performance. In: Proc. SAG 2006, Vancouver, B.C., Canada. pp. 217–232.
Wakefield, B. J., Lindner, B. S., McCoy, J. T., Auret, L., 2018. Monitoring of a simulated milling circuit: fault diagnosis and economic impact. Minerals Eng. 120, 132–151.
Wei, D., Craig, I. K., 2009. Grinding mill circuits - A survey of control and economic concerns. Int. J. Mineral Process. 90 (1-4), 56–66.
Yang, J., Li, S., Chen, X., Li, Q., 2010. Disturbance rejection of ball mill grinding circuits using DOB and MPC. Powder Tech. 198, 219–228.
Zhou, P., Lu, S., Yuan, M., Chai, T., 2016. Survey on higher-level advanced control for grinding circuits operation. Powder Tech. 288, 324–338.